# Well-defined polyester-grafted silica nanoparticles for biomedical applications: Synthesis and quantitative characterization

Prescillia Lagarrigue, Jérémy Soulié, David Grossin, Agnès Dupret Bories, Christèle Combes, Vincent Darcos

# Well-defined polyester-grafted silica nanoparticles for biomedical applications: Synthesis and quantitative characterization

Prescillia Lagarrigue [a,c,*], Jérémy Soulié [a], David Grossin [a], Agnès Dupret-Bories [a,b], Christèle Combes [a], Vincent Darcos [c,**]

[a] CIRIMAT, Université de Toulouse, CNRS, Toulouse INP - ENSIACET, 31030, Toulouse, France
[b] Service de Chirurgie ORL et Cervico-faciale, IUCT-Oncopole, 31100, Toulouse, France
[c] IBMM, Univ Montpellier, CNRS, ENSCM, 34093, Montpellier, France

ARTICLE INFO

*Keywords:*
Polyesters
Silica nanoparticles
Grafted nanoparticles

ABSTRACT

Polyester-based composites with silica nanoparticles fillers are promising candidates as biomaterials due to improved mechanical and biological properties. However, nanofillers use generally leads to an inhomogeneous distribution inside the polymer matrix because of agglomeration, decreasing composites overall performances. In view of improving nanofillers dispersion, we developed a synthesis and characterization method to design poly(D,L-lactide)-grafted silica nanoparticles using "grafting to" method and to quantify the amount of grafted poly(D,L-lactide). Firstly, well-defined *N*-hydroxysuccinimide ester poly(D,L-lactide)s were synthesized through a new pathway. Then, amino-functionalized silica nanoparticles were grafted with those customized polyesters yielding an amide covalent bond between both reagents. Such PDLLA-grafted nanoparticles were precisely characterized and the grafting amount was quantified using a dual approach based on TGA and FTIR analysis. The synthesis and the characterization methods developed constitute a robust and reproducible way to design well-defined polymer-grafted silica nanoparticles that could be used as nanofillers in polymer matrix nanocomposites for biomedical applications.

## 1. Introduction

Bone defects and related diseases remain a challenge for surgeons, and represent half of chronic diseases for people over 50. Defects resulting in fractures and/or trauma are mainly caused by traffic accident, falls, aged fragility and tumor resections [1–3]. For small size defects, bones are able to regenerate, but, for critical size defects, bone regenerative properties are not sufficient to allow a global reparation. Autologous bone grafting is the method currently used to treat critical size bone defects. This procedure presents disadvantages including secondary damages to the donor site, such as infections or morbidity, and difficulties in shaping the bone graft to perfectly fill with initial defect [3].

Composites biomaterials for tissue engineering such as scaffolds [4–8] are an interesting solution for bone defects treatment by mimicking bone structure, providing a 3D environment to promote cell adhesion, proliferation and differentiation, improving their global mechanical behavior and presenting tailored biodegradability. These inorganic-organic composites combine toughness of polymeric matrices including natural or synthetic polymers [9–11] and compressive strength of inorganic fillers like apatite [12], Bioglass® [13] or silica [14,15].

In the biomedical field, synthetic polymers commonly used as composite matrix are aliphatic polyesters such as poly(lactide) (PLA), poly(glycolide) (PGA) and a copolymer combining the two previous ones, poly(lactide-*co*-glycolide) (PLGA) [4,10]. The physical and mechanical properties of these polymers can be changed by varying the molecular weight or comonomer composition, which in turn, control the polymers biocompatibility, degradation rate, cell attachment and cell growth [4,10,16–18]. More particularly, poly(D,L-lactide) (PDLLA) is a versatile polymer for biomedical applications such as composite matrix because of its high and tunable degradation rate, between 2 and 12 months [16–18].

Inorganic filler addition inside polymer matrix also improve

* Corresponding author.
** Corresponding author.
*E-mail addresses:* prescillia.lagarrigue@toulouse-inp.fr (P. Lagarrigue), jeremy.soulie@ensiacet.fr (J. Soulié), david.grossin@ensiacet.fr (D. Grossin), dupret-bories.agnes@iuct-oncopole.fr (A. Dupret-Bories), christele.combes@ensiacet.fr (C. Combes), vincent.darcos@umontpellier.fr (V. Darcos).

https://doi.org/10.1016/j.polymer.2020.123048

bioactivity, mechanical and structural properties of composite scaffolds. Silica nanoparticles are interesting biomedical composite fillers for several reasons. Firstly, silicates are essential for metabolic processes, formation and calcification of bone tissue as they stimulate collagen I formation and osteoblastic differentiation [19,20]. In addition, when used as fillers, silica nanoparticles are known to improve mechanical and structural properties of the final material [21–24]. However, the introduction of nanoparticle fillers in polymer matrix raises a challenge in term of homogeneity. In fact, nanoparticles form agglomerates in solubilized polymer matrix, which limit their homogeneous dispersion inside the final composite and thus decrease the overall performances of the material [21,25]. This heterogeneous distribution may result in preferential zones degradation and mechanical weakening of the scaffold. Thus, a method that provides homogeneous dispersion of nanofillers is necessary to obtain uniform properties of biomaterials [26].

To improve nanoparticles distribution in the polymer matrix during mixing or material processing, different studies propose a chemical modification of silica nanoparticle surface, previously treated with silane coupling agent such as 3-aminopropyltriethoxysilane [21,27–30], with polymer leading to polymer-grafted particles. For the covalent grafting of polymer on the surface of nanofillers, two approaches are available: “grafting from” (GF) and “grafting to” (GT) methods. The GF method has been more widely studied in recent researches than GT method. In fact, recent studies show that GF method (in situ melt polycondensation [31–33], direct ring opening polymerization using particles as macroinitiator [34,35]) presents higher grafting density than the GT method that is limited by steric hindrance of polymer chains during the grafting process. GT, however, allows a more precise control of the molecular weight and the architecture of grafted polymer chains [36]. This is a key feature as one of the most relevant parameter for homogeneous nanoparticles dispersion is the grafted/free chains mass ratio [37]. Indeed, the latter enables to manage the arrangement of the grafted nanoparticles inside the matrix to be either large aggregates or as individual nanoparticles dispersion. The composite nanoscale microstructure strongly affects the mechanical and/or degradation properties.

Studies focused on GT method of PLA polymers on silica nanoparticles have found that PLLA grafted nanoparticles are interesting nanofillers for PLLA composites. Yan et al. [38] performed PLLA oligomers GT functionalization of silica nanoparticles by condensation reaction without any catalyst and Wu et al. [39] used the GT method to successfully graft PLLA to the silica surface using an amidation reaction. Other authors propose further PLLA or silica modification to improve PLLA grafting to silica nanoparticles using 2,4-diisocyanatotoluene (TDI) [35,40]. However, from this review of literature, we note that no study has reported on silica nanoparticles grafted with PDLLA and its characterization. The aim of this study is to develop such nanosystems using “grafting to” method, and to quantify precisely the grafting.

In this work, we provide a detailed report of the synthesis of inorganic particles functionalized with degradable polymers using a “grafting to” approach. First, the synthesis and characterization of poly(D,L-lactide)s and their customization leading to *N*-hydroxysuccinimide ester poly(D,L-lactide)s are discussed. Then, silica nanoparticles synthesis using a modified Stöber process [41] and their surface functionalization with silane coupling agent are presented. In the last step, poly(D,L-lactide)-grafted silica nanoparticles elaboration by covalent coupling reaction of both precursors is demonstrated. The full characterization of those systems before and after covalent coupling mainly using NMR spectroscopy, SEC, TEM, DLS, TGA allows to verify that PDLLA chains are grafted on silica nanoparticles surface and a dual approach permits the grafting quantification using FTIR and TGA analysis. The results of this study could have greater implication in the development of PDLLA/silica nanoparticles biomedical composite scaffolds, using PDLLA-grafted silica nanoparticles as nanofillers, for bone defects treatment.

## 2. Materials and methods

### 2.1. Materials

D,L-lactide was purchased from Corbion Purac (PURASORB® DL Goerinchem). 4-(dimethylamine)pyridine (DMAP), stannous 2-ethyl hexanoate ($Sn(Oct)_2$), *N,N′*-dicyclohexyl carbodiimide (DCC), succinic anhydride (SA), tetraethyl orthosilicate (TEOS), ammonium hydroxide solution (28–30% $NH_3$ basis), 3-aminopropyl triethoxysilane 99% (APTES), methanol, ethanol, 1,4-dioxane, acetone, acetonitrile, *n*-heptane and hydrochloric acid were obtained from Sigma-Aldrich and were used without any further purification. *N*-hydroxysuccinimide (NHS) was purchased from ACROS. Dichloromethane, toluene and *N,N*-dimethylformamide (DMF, Sigma-Aldrich) were dried over calcium hydride for 24 h and distilled. Benzyl alcohol and triethylamine (TEA) (Sigma-Aldrich) were dried over potassium hydroxide for 24 h and distilled. Ultrapure water with resistivity of 18 MΩ.cm was produced thank to a Millipore Milli-Q water system. Pre-wetted RC tubing dialysis membranes (1 kD) were purchased from Spectrumlabs.

### 2.2. Synthesis and grafting

#### 2.2.1. Synthesis of poly(D,L-lactide) (PDLLA-OH)

PDLLA-OH was synthesized by ring-opening polymerization of D,L-lactide using standard Schlenk technique under argon atmosphere with benzyl alcohol (BnOH) as initiator and $Sn(Oct)_2$ as catalyst. Typically, to obtain PDLLA-OH with a molecular weight of $M_n$ 2200 g.mol$^{-1}$, 5 g of D,L-lactide (34.7 mmol), 94 mg of $Sn(Oct)_2$ (0.23 mmol), 250 mg of benzyl alcohol (2.31 mmol), and 10 mL of anhydrous toluene were placed in an oven dried Schlenk tube closed with a rubber septum. The solution was further degassed by three freeze pump-thaw cycles, and polymerization was performed overnight in an oil bath at 80 °C, with stirring and under an argon atmosphere. The polymerization was quenched with 3 drops of 1 N hydrochloric acid in methanol. After cooling down at room temperature, the mixture was poured in cold *n*-heptane. The precipitated polymer was collected by filtration and dried under vacuum (yield 98%).

$^1$H NMR (300 MHz, $CDCl_3$, $\delta$ (ppm)): 7.3 (m, $C_6H_5$); 5.11 (m, C*H*–$CH_3$); 4.33 (q, $(CH_3)$C*H*–OH); 1.52 (m, CH–C*H*$_3$). $M_{n,NMR}$ = 2400 g.mol$^{-1}$, $M_{n,SEC}$ = 3000 g.mol$^{-1}$, $Đ$ = 1.16.

#### 2.2.2. Synthesis of N-hydroxysuccinimide ester poly(D,L-lactide) (PDLLA–COO–NHS)

The synthesis of PDLLA–COO–NHS was performed in two steps. First, carboxy-terminated PDLLA were synthesized according to a known procedure described by Lee et al. [42]. In a dried round bottom flask equipped with a condenser, 2 g of PDLLA-OH (0.91 mmol, $M_n$ 2200 g.mol$^{-1}$), dimethylaminopyridine (22 mg, 0.18 mmol), and succinic anhydride (909 mg, 9.1 mmol) were dissolved in 25 mL of 1,4-dioxane at 100 °C. Then, triethylamine (918 mg, 9.1 mmol) was added. The solution was stirred at 100 °C for 48 h, cooled, and the solvent removed under reduced pressure. Dichloromethane (50 mL) was added to the residue, and the mixture was extracted with three 50 mL portions of saturated sodium chloride solution. The organic phase was then dried over $MgSO_4$ and the solvent removed under reduce pressure.

In a second step, carboxy-terminated PDLLA were activated with NHS. To a solution of the resulting polymer in 10 mL of anhydrous dichloromethane cooled to 0 °C, NHS (145 mg, 1.26 mmol) was added slowly. Then, a solution of *N,N′*-dicyclohexyl carbodiimide (DCC) (260 mg, 1.26 mmol) in 5 mL of anhydrous dichloromethane was added dropwise. The reaction was performed during 72 h at room temperature. Then the flask was immersed in an ice bath to stop the reaction. Dichloromethane was removed under reduced pressure. Acetonitrile (50 mL) was added to the residue and the flask was placed in a freezer for 6 h to precipitate the formed dicyclohexylurea (DCU). The solution was then centrifuged three times 10 min at −5 °C and 5500 rpm to evacuate

the precipitated DCU. The resulting solution was dialyzed in tubing dialysis membrane (1 kD) and placed under stirring in a mix of methanol and acetone (50:50) during 2 days. The solvent was renewed twice a day. Finally the solvent of dialyzed solution was removed under reduced pressure and the resulting polymer was dried under vacuum.

$^1$H NMR (300 MHz, $CDCl_3$, $\delta$ (ppm)): 7.3 (m, $C_6H_5$); 5.11 (m, C*H*–$CH_3$); 2.98 (d, COO–C*H*$_2$–$CH_2$–COO); 2.83 (m, COO–$CH_2$–C*H*$_2$–COO + CO–C*H*$_2$–C*H*$_2$–CO); 1.52 (d, CH–C*H*$_3$).

### 2.2.3. Synthesis of silica nanoparticles (Np)

Silica nanoparticles were synthesized using a modified Stöber process through a sol gel route [41]. Firstly, 100 mL of absolute ethanol were mixed with 10.8 mL of MilliQ water and 3.9 mL of ammonium hydroxide under vigorous stirring during 15 min. Then, 6.3 mL of TEOS was added to the solution. After 17 h, the obtained suspension was centrifuged at 5500 rpm during 10 min and the solid pellet of particles was then frozen with liquid nitrogen and freeze-dried for 3 days. Approximately 1.7 g of silica nanoparticles were obtained at the end of this process.

### 2.2.4. Nanoparticle surface functionalization (Np-$NH_2$)

Amino functionalized Np were prepared according to a modified procedure described by El Fiqi et al. [27,43]. 700 mg of Np were added to 50 mL of distilled toluene in an oven dried Schlenk tube closed with a rubber septum. After dispersion of the nanoparticles with an ultrasonic probe (Bioblock Scientific Vibracell 75,115, 5 min, amplitude 60%), the Schlenk tube was put under argon atmosphere and under vigorous stirring in an oil bath at 80 °C. Then, APTES (7 mL, 29.9 mmol) was added under an inert atmosphere with a syringe through the rubber septum. The suspension was heated at 80 °C overnight. Then, the suspension was centrifuged in fluorinated ethylene propylene tubes (FEP) during 10 min at 5000 rpm. The nanoparticle pellets were washed three times with distilled toluene (dispersion with an ultrasonic probe and centrifugation) and dried at 80 °C under vacuum during 24 h. This protocol led to about 553 mg of amino functionalized silica nanoparticles.

### 2.2.5. Synthesis of PDLLA-grafted silica nanoparticles (Np-PDLLA)

100 mg of amino-functionalized nanoparticles (Np-$NH_2$) were dispersed with an ultrasonic probe (10 min, amplitude 60%) in 5 mL of distilled DMF in an oven dried Schlenk tube. Then, triethylamine was added (100 µL). The Schlenk tube was placed in an oil bath at 65 °C under argon atmosphere and stirring. Then, a solution of PDLLA–COO–NHS (233 mg, $M_n$ = 5200 g.mol$^{-1}$) in 5 mL of DMF was transferred dropwise into the Schlenk tube and the reaction was left for 24 h at 65 °C. The solvent was then removed by centrifugation. The residue was washed twice with 10 mL of toluene and twice with 10 mL of ethyl acetate (dispersion and centrifugation) to evacuate the remaining free PDLLA chains. The remaining nanoparticles were then dried under vacuum during 2 days, leading to approximately 84 mg of PDLLA-grafted silica nanoparticles.

## 2.3. Characterization of structure and properties

### 2.3.1. Polymer characterization

$^1$H NMR spectra were recorded on a Bruker spectrometer (AMX300) operating at 300 MHz in $CDCl_3$ as solvent. The chemical shifts were referenced to the peak of residual non-deuterated solvents.

Average molecular weights ($M_n$) and dispersities ($Đ$) were determined using size exclusion chromatography (SEC) on a Shimadzu Prominence system (*Shimadzu* Corp, Kyoto, Japan). This system is equipped with a PLgel MIXED-C guard column (Agilent, 5 µm, 50 × 7.5 mm), two mixed medium columns PLgel MIXED-C (5 µm, 300 × 7.8 mm) and a Shimadzu RI detector 20-A. The mobile phase was THF with a flow of 1 mL.min$^{-1}$ at 35 °C. Polystyrene standards were used for calibration and polymers characteristics obtained expressed according to those standards.

MALDI-TOF mass spectrometry was performed on a Bruker RapifleX equipped with a $N_2$ laser (337 nm) in the reflector mode and at 20 kV acceleration voltage. The analysis were run using t-2-[3-(4-*t*-butylphenyl)-2-(methyl-2-propenylidene)] malononitrile (DCTB) as matrix with sodium iodide (NaI) for ion formation.

### 2.3.2. Particle characterization

Transmission electron microscopy (TEM) was used to image initial nanoparticles and PDLLA-grafted nanoparticles. Samples were dispersed in ethanol (0.5 mg mL$^{-1}$) and deposited on 300 mesh copper TEM grids. Imaging was performed on JEOL 1200 EXII TEM using an operating voltage of 120 kV. Multiple areas of each grid were analyzed and, for nanoparticle size determination, at least 100 particles were measured to calculate mean particle diameter ($D_{av}$) and standard deviation by image processing (ImageJ, with "Analyze particles" tool).

Nanoparticle mean hydrodynamic diameter ($Z_{av}$) of initial nanoparticles and PDLLA-grafted nanoparticles was determined using dynamic light scattering (DLS, Malvern Instrument Zetasizer Nano-ZS) after dilution of the samples in ethanol (0.5 mg.mL$^{-1}$) and sonication during 10 min. The mean hydrodynamic radius and polydispersity index (*PdI*) were evaluated after 3 runs for each sample.

Nanoparticle specific surface area (SSA) was estimated according single point Brunauer-Emmett-Teller (BET) method using $N_2$ adsorption, on a Monosorb Quantachrome device. Measurements were performed five times on initial silica nanoparticles after degassing at 100 °C overnight.

The electrical surface charge properties of the initial, amino-functionalized and PDLLA-grafted nanoparticles were investigated by Zeta ($\zeta$) potential measurements using a Malvern instrument Zetasizer Nano-ZS. The measurements were performed at 25 °C in distilled water, after dispersion of the sample with an ultrasonic probe (0.1 mg.mL$^{-1}$), with an applied field strength of 20 V.cm$^{-1}$. Mean zeta potential value and standard deviation were evaluated on 3 measurements of 12 runs for each sample.

Cross polarization magic angle spinning $^{29}$Si solid state nuclear magnetic resonance spectroscopy analysis (CP-MAS $^{29}$Si NMR

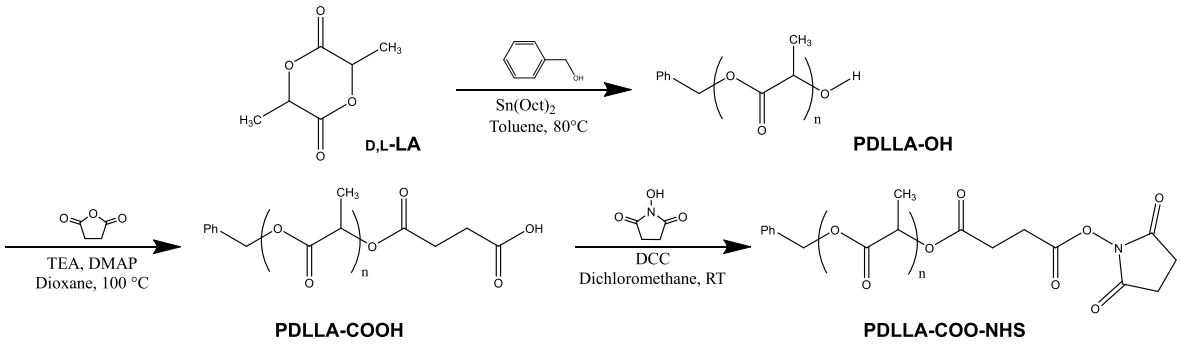


**Scheme 1.** Synthetic pathway for the preparation of *N*-hydroxysuccinimide ester poly(D,L-lactide).

**Table 1**
Characteristics of poly(D,L-lactide) synthesized by ring-opening polymerization.

| | $[D,L\text{-La}]_0/[BnOH]_0/[Sn]_0$ [a] | $M_{n,th}$ (g.mol$^{-1}$) | $M_{n,NMR}$ [b] (g.mol$^{-1}$) | $M_{n,SEC}$ [c] (g.mol$^{-1}$) | $Đ$ [c] |
|---|---|---|---|---|---|
| $PDLLA_{2.2K}$–OH | 15/1/0.1 | 2200 | 2400 | 3000 | 1.16 |
| $PDLLA_{5.2K}$–OH | 35/1/0.1 | 5200 | 4900 | 7500 | 1.10 |

[a] Conditions of ROP: $[D,L\text{-La}]_0 = 3.47$ mol.L$^{-1}$, T = 80 °C, solvent: toluene.
[b] Determined by $^1$H NMR spectroscopy in $CDCl_3$.
[c] Determined by SEC in THF using PS standards.

spectroscopy) was performed to characterize the surface functionalization of nanoparticles with amine groups using a VNMRS 400 MHz VARIAN spectrometer, with a "Wide Bore" magnet (9.4 T), a T3 VARIAN probe and 7.5 mm zirconia rotors. Samples were analyzed at a contact time of 5 ms and recycle time of 5 s, with a rotation speed of 5 kHz. Calibration of the analysis was based on Q8M8H (octakis(dimethylsiloxy)octasilsesquioxane) as secondary reference. The acquisition window was of 50 kHz and the line broadening was 50 Hz.

Fourier transformed infrared (FTIR) spectroscopy analyses were run on sample in KBr pellet in transmission mode using a Nicolet 5700 spectrometer (400-4000 cm$^{-1}$, 64 scans, resolution 4 cm$^{-1}$). We prepared 12 mm pellets by mixing 1 mg of nanoparticles or polymer with 300 mg of KBr pressed at 8 tons pressure.

Thermogravimetric analyses (TGA) of the different constituents were recorded using a Setaram instrument (Setsys Evolution System) from 25 °C to 700 °C with a heating rate of 5 °C per minute under argon flow, with a dwell of 30 min at 25 °C.

## 3. Results and discussion

### 3.1. Synthesis of poly(D,L-lactide) (PDLLA-OH)

Well-defined poly(D,L-lactide) with carboxylic end-groups activated by NHS, named PDLLA–COO–NHS, were synthesized in 3 steps by combining ring-opening polymerization (ROP) and conjugation chemistry (Scheme 1).

Firstly, PDLLA-OHs were prepared by ROP of D,L-lactide using tin octanoate ($Sn(Oct)_2$) as catalyst and benzylic alcohol as initiator. Table 1 shows the characteristics of two PDLLA-OH ($PDLLA_{2.2K}$–OH and $PDLLA_{5.2K}$–OH) using two different D,L-lactide/initiator feed ratios (15 and 35). The conversion was quantitative in both cases.

(Fig. 1, A) shows the $^1$H NMR spectrum of PDLLA-OH. The peaks at $\delta$ 5.11 and 1.52 ppm were associated to the polymer backbone. The peak at $\delta$ 7.3 ppm was correlated to the aromatic protons of the initiator. The hydroxyl methine end-group appeared at $\delta$ 4.33 ppm as a weak resonance. The molecular weights determined by $^1$H NMR spectroscopy ($M_{n,NMR}$) were calculated from the relative intensity of NMR signals of the lactic acid units ($\delta$ 5.11 ppm and $\delta$ 4.33 ppm) and the phenyl group ($\delta$ 7.3 ppm), following Eq. (1).

$$M_{n,NMR} = 108 + \frac{72 \times (I_b + I_d)}{1/5 I_a} \quad (1)$$

where 108 and 72 are the molar masses (g.mol$^{-1}$) of benzyl alcohol and lactic acid units respectively. $I_a$, $I_b$ and $I_d$ are the integration values of $^1$H NMR signal of the phenyl end group (a) at $\delta$ 7.3 ppm, the polymer backbone (b) at $\delta$ 5.11 ppm, and the one of hydroxyl methine end group (d) at $\delta$ 4.33 ppm.

As reported in Table 1, molecular weights $M_{n,NMR}$ ($PDLLA_{2.2K}$–OH, $M_{n,NMR}$ = 2400 g.mol$^{-1}$; $PDLLA_{5.2K}$–OH, $M_{n,NMR}$ = 4900 g.mol$^{-1}$) are close to the targeted value ($PDLLA_{2.2K}$–OH, $M_{n,th}$ = 2200 g.mol$^{-1}$; $PDLLA_{5.2K}$–OH, $M_{n,NMR}$ = 5200 g.mol$^{-1}$). The molecular weights estimated by SEC using PS standards ($PDLLA_{2.2K}$–OH, $M_{n,SEC}$ = 3000 g.mol$^{-1}$; $PDLLA_{5.2K}$–OH, $M_{n,SEC}$ = 7500 g.mol$^{-1}$) are higher than those determined by $^1$H NMR spectroscopy. Indeed, it is well-known that PLA molecular weight determined by SEC with PS standards are overestimated [44,45]. To conclude, the two different polymers were achieved with a good control of $M_n$ and low dispersities ($PDLLA_{2.2K}$–OH, $Đ$

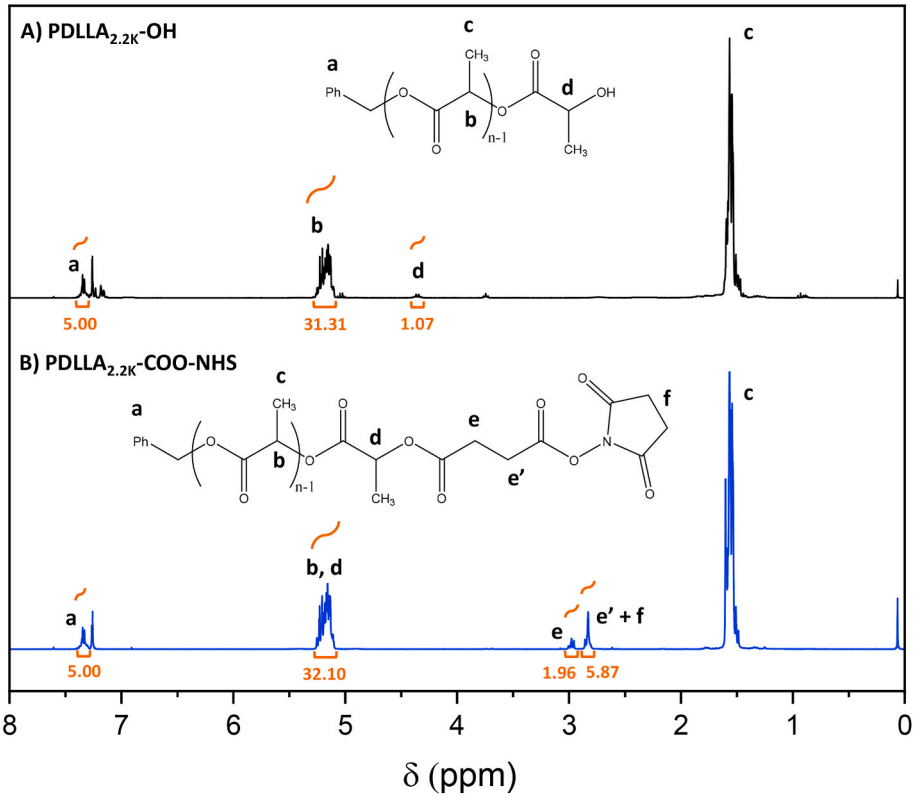


**Fig. 1.** $^1$H NMR spectrum of A) $PDLLA_{2.2K}$–OH and B) $PDLLA_{2.2K}$–COO–NHS in $CDCl_3$.

**Table 2**
Characteristics of *N*-hydroxysuccinimide ester poly(D,L-lactide).

| | Starting polymer | Functionalization ratio τ[a] | $M_{n,NMR}$[a] (g.mol$^{-1}$) | $M_{n,SEC}$[b] (g.mol$^{-1}$) | $Đ$[b] |
|---|---|---|---|---|---|
| $PDLLA_{2.2K}$–COO–NHS | $PDLLA_{2.2K}$–OH | 98% | 2600 | 3600 | 1.12 |
| $PDLLA_{5.2K}$–COO–NHS | $PDLLA_{5.2K}$–OH | 93% | 5100 | 8000 | 1.13 |

[a] Determined by $^1$H NMR spectroscopy in $CDCl_3$.
[b] Determined by SEC in THF using PS standards.

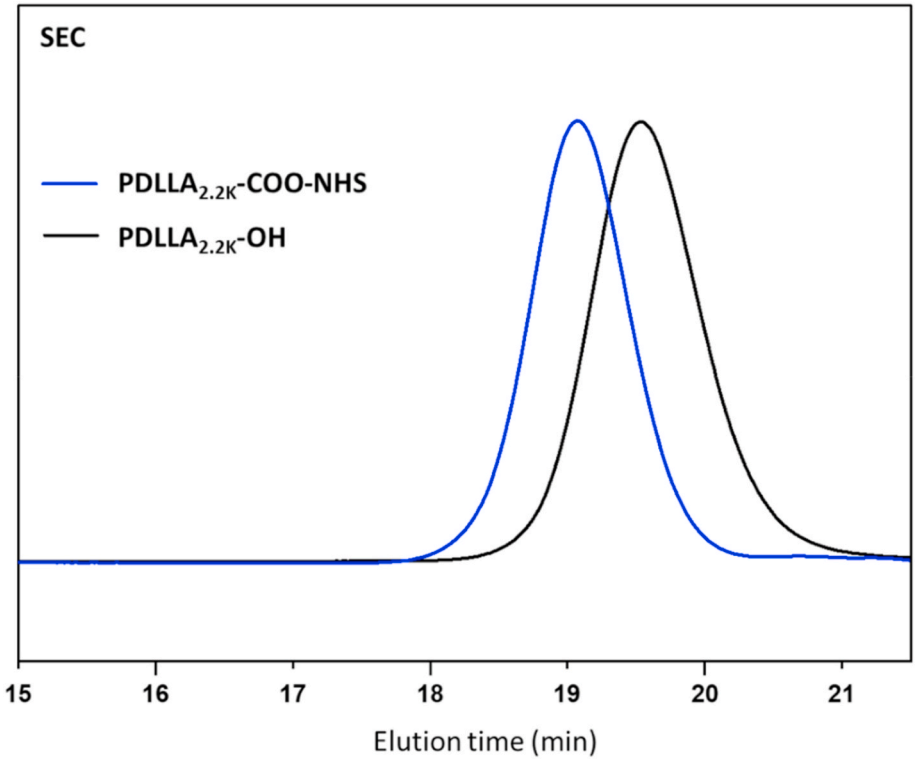


**Fig. 2.** SEC traces of $PDLLA_{2.2K}$–OH and $PDLLA_{2.2K}$–COO–NHS in THF.

= 1.16 and $PDLLA_{5.2K}$–OH, $Đ$ = 1.10), which prove the well-controlled polymerization process.

### 3.2. Synthesis of N-hydroxysuccinimide ester poly(D,L-lactide) (PDLLA–COO–NHS)

In a second step, PDLLA-COOH were prepared by the reaction of PDLLA-OH with succinic anhydride in the presence of DMAP and TEA used as catalysts (Scheme 1). Then, the carboxyl moiety of PDLLA-COOH was activated by reaction with NHS in presence of DCC, yielding PDLLA–COO–NHS polymers ($PDLLA_{2.2K}$–COO–NHS and $PDLLA_{5.2K}$–COO–NHS) that would be able to react with functionalized silica nanoparticles. NHS ester is probably the most common activation chemical for producing reactive acylating agents. Fig. 1 shows the $^1$H NMR spectra of $PDLLA_{2.2K}$–OH and $PDLLA_{2.2K}$–COO–NHS. $^1$H NMR spectroscopy data confirm the functionalization of the PDLLA-OH in PDLLA–COO–NHS. The terminal methine proton (Fig. 1 A, peak d) disappeared after the reaction with succinic anhydride and NHS. A triplet appears at $\delta$ 2.98 ppm corresponding to two hydrogen atoms from succinic anhydride (peak e) and a multiplet appears at $\delta$ 2.83 ppm corresponding to an overlap of two hydrogen atoms from succinic anhydride (peak e') and the four hydrogen atoms from terminal NHS (peak f). The functionalization ratio τ of the hydroxyl end-groups, determined by $^1$H NMR spectroscopy, is almost quantitative for $PDLLA_{2.2K}$–OH (τ = 98%, Fig. 1) and functionalization rate is good for $PDLLA_{5.2K}$–OH (τ = 93%, Figure S1). Functionalization ratios were evaluated by comparing the peak area of succinic anhydride and NHS hydrogen overlap (f + e') with the peak area of the characteristic PDLLA multiplet at 5.11 ppm (b). The molecular weights ($M_{n,NMR}$) were determined using relative intensity of $^1$H NMR signals of phenyl group (a), lactic acid units (b,d) and functionalization end groups (e, e' + f) and following Eq. (2).

$$M_{n,NMR} = 108 + \frac{72 \times (I_b + I_d)}{1/5 I_a} + 197 \times \tau \quad (2)$$

where 108, 72 and 197 are the molar masses (g.mol$^{-1}$) of benzyl alcohol, lactic acid units and functional end-group respectively. $I_a$ and ($I_b + I_d$) are the integration values of $^1$H NMR signal of the phenyl end-group (a) at $\delta$ 7.3 ppm, and the polymer backbone (b,d), at $\delta$ 5.11 ppm. τ is the functionalization ratio.

The molecular characteristics of the two customized polymers $PDLLA_{2.2K}$–OH and $PDLLA_{5.2K}$–OH are reported in Table 2. For the end-functional polyesters, $^1$H NMR spectroscopy and SEC analysis results (Fig. 2 and Figure S2) both showed a slight increase of polymers molecular weight ($PDLLA_{2.2K}$–COO–NHS: $M_{n,NMR}$ = 2600 g.mol$^{-1}$ and $M_{n,SEC}$ = 3600 g.mol$^{-1}$; $PDLLA_{5.2K}$–COO–NHS: $M_{n,NMR}$ = 5100 g.mol$^{-1}$ and $M_{n,SEC}$ = 8000 g.mol$^{-1}$). The SEC dispersities remained similar ($PDLLA_{2.2K}$–COO–NHS, $Đ$ = 1.12 and $PDLLA_{5.2K}$–COO–NHS, $Đ$ = 1.13) in comparison with starting polymers. Those results indicate that no chain cleavage occurred during the chemical modification of PDLLA-OH.

The initial polymer $PDLLA_{2.2K}$–OH and customized one $PDLLA_{2.2K}$–COO–NHS were also characterized by MALDI-TOF mass spectrometry (Figure S3). Using MALDI-TOF, complete structural

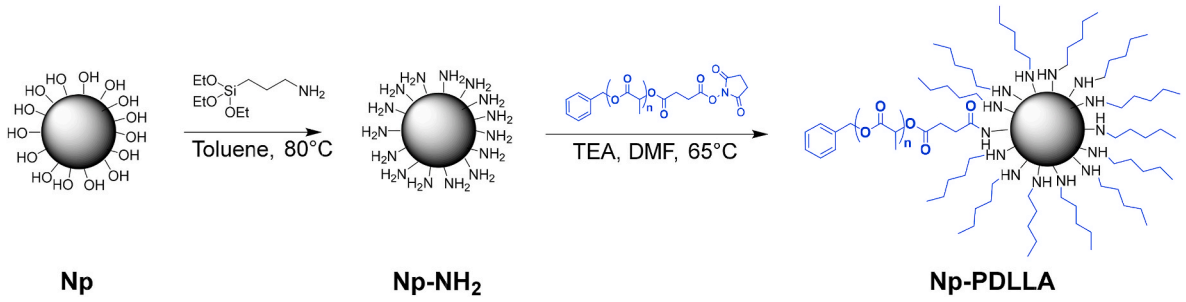


**Scheme 2.** Illustration of silica nanoparticle modifications: Nanoparticle surface functionalization with amine groups using APTES and PDLLA–COO–NHS "grafting onto" functionalized nanoparticle surface.

analysis with the verification of the functionalization could be performed. This analysis gave the distribution of polymer chains based on their $m/z$ ratio that can be linked to the chain molecular weight. The distributions obtained for $PDLLA_{2.2K}$–OH and $PDLLA_{2.2K}$–COO–NHS present Gaussian curves proving a good control of the reaction. In the case of $PDLLA_{2.2K}$–OH, the maximal peak at $m/z = 2291.7$ is close to the molecular weight found with $^1$H NMR spectroscopy ($M_{n,NMR} = 2400$ g. mol$^{-1}$) and corresponds to the expected degree of polymerization of 15. In the case of $PDLLA_{2.2K}$–COO–NHS, the maximal peak is at $m/z = 2488.7$, the difference between this value and the one of the maximal $PDLLA_{2.2K}$–OH peak corresponds exactly to the molecular weight of the grafted group on the $PDLLA_{2.2K}$–OH hydroxyl terminal end-group. On Figure S3 A and B, we can see that the difference between two high intensity peaks is of 144.04 which corresponds to the weight of a D,L-lactide monomer unit. The presence of less intense peaks separated from high intensity peaks by 72.02, highlights *trans*-esterification reactions during the polymer synthesis. MALDI-TOF spectrometry was only performed on $PDLLA_{2.2K}$–OH, as this analysis is less relevant for higher molecular weights.

It's interesting to notice that Lee et al. already described the functionalization of poly(L-lactide) polymers with carboxylic acid end-groups on high molecular weight polymers [42]. Lim et al. described modification of poly(vinyl alcohol) with a two-steps process using SA and NHS/DCC to graft tyramine [46]. However, to the best of our knowledge, the synthesis of well-defined PDLLA–COO–NHS using a two-steps process involving succinic anhydride and NHS/DCC and its fine characterization has never been described so far. Those customized polymers presenting an activated carboxylic acid end-group present high reactivity with amine groups, thus permitting covalent grafting on amino-functionalized nanoparticles.

### 3.3. Synthesis of silica nanoparticles (Np)

Silica nanoparticles were synthesized by sol-gel route, adding TEOS in a mixed solution containing pure ethanol, ammonium hydroxide and water. The basic pH due to ammonium hydroxide, allowed the formation of spherical silica particles by hydrolysis and condensation of TEOS silanol groups [47]. As previously stated, it is well-known that particle size can be tuned in Stöber-derived processes by varying several parameters such as TEOS concentration or pH [41]. In the present study, parameters have been fixed to obtain monodisperse Np of several hundred nanometers; the latter will be used to demonstrate the proof of concept of covalent grafting with PDLLA. Moreover, in view of bone substitution applications, such Np diameters could prevent the particle uptake through biological membrane. After the reaction, the suspension was centrifuged and the collected packed nanoparticles was then freeze-dried during 3 days. The centrifugation and drying processes are key steps to limit condensation reaction between particles and consequently agglomeration phenomena that occur in presence of water [21]. In order to obtain reactive silica nanoparticles and allow polymer grafting onto its surface, APTES was used to functionalize silica surface with amine groups by hydrolysis (Scheme 2).

The size of initial silica Np was analyzed both by TEM followed by image processing and DLS measurements. TEM observations (Fig. 3) clearly show spherical and homogeneous size of silica Np. Image processing, with ImageJ, on at least 100 Np gave an average diameter of $357 \pm 19$ nm with a low polydispersity index ($PdI = 0.003$) proving that the reaction is well controlled. DLS measurements performed on a suspension of silica Np in pure ethanol gave information on the hydrodynamic diameter ($Z_{av}$). For silica Np, we obtained a $Z_{av}$ of $383 \pm 1$ nm with a low polydispersity index (0.096) (Table 3), confirming a narrow polydispersity of the Np and a good size control during Stöber process. As DLS measures hydrodynamic diameter and not particles diameter, it is obvious that DLS measurements over evaluate the Np diameter.

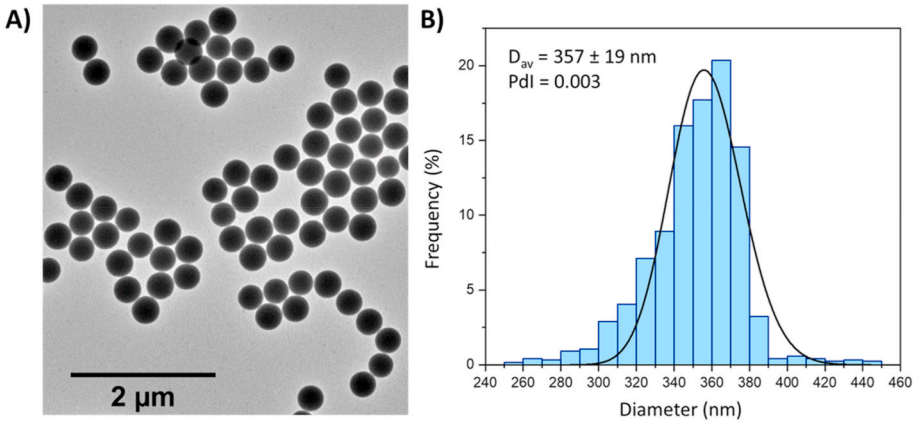


**Fig. 3.** A) TEM image and B) size distribution of initial silica nanoparticles (Np).

**Table 3**
Size characteristics of initial nanoparticles (Np) and PDLLA-grafted nanoparticles (Np-PDLLA).

| | TEM | | DLS | | BET |
|---|---|---|---|---|---|
| | $D_{av} \pm \sigma$ (nm) | PdI | $Z_{av} \pm \sigma$ (nm) | PdI | SSA $\pm \sigma$ ($m^2.g^{-1}$) |
| Np | 357 ± 19 | 0.003 | 383 ± 1 | 0.096 | 14.2 ± 0.1 |
| Np-PDLLA | 359 ± 24 | 0.004 | 890 ± 38 | 0.312 | |

**Table 4**
Zeta-potential measurements of initial nanoparticles (Np), amine-functionalized nanoparticles (Np-$NH_2$), and PDLLA-grafted nanoparticles (Np-PDLLA).

| | ζ-potential ± σ (mV) |
|---|---|
| Np | −32 ± 2 |
| Np-$NH_2$ | 14 ± 1 |
| Np-PDLLA | −18 ± 1 |

Specific surface area (SSA) of initial Np, 14.2 ± 0.1 $m^2.g^{-1}$, was determined by single point BET method using $N_2$ adsorption and is in the same range than results found in the literature [48].

### 3.4. Nanoparticle surface functionalization (Np-$NH_2$)

Silica Np surface was then treated with APTES performing a coupling chemical reaction between Np surface hydroxyl groups and APTES ethoxy groups. Z-potential of silica Np (Table 4) was measured before and after treatment with APTES to check the surface functionalization. Initial silica Np presented a negative ζ-potential (−32 ± 2 mV) which can be explained by the presence of hydroxyl group at their surface. After APTES treatment, the amino-functionalized Np presented a positive ζ-potential (14 ± 1 mV), due to the modification of hydroxyl groups by APTES, leading to $NH_2$ surface groups. This modification of the ζ-potential value sign attests the surface modification of the Np with amino groups and was already described in the literature [28,43].

Functionalization of Np surface with APTES was also investigated by $^{29}$Si CP-MAS solid-state NMR spectroscopy. This non quantitative analysis allowed the identification of the various species of Si units forming the Np network. Fig. 4 shows the $^{29}$Si CP-MAS NMR spectrum of Np-$NH_2$ with a main contribution between −125 ppm and −80 ppm, which is related to the overlapping contributions of the different siloxane groups, $Q^n$ units representing the number of Si–O–Si bonds per silicon atom. The resonance at −107.9 ppm is ascribed to $Q^4$ units; the one at −99.1 ppm corresponds to $Q^3$ units and the last one at −91.6 ppm to $Q^2$ units. The second resonance between −75 ppm and −50 ppm is composed of two $T^n$ contributions: −64.9 ppm ($T^3$) and −57.7 ppm ($T^2$) which correspond to grafted species and represent the number of Si–O–Si bonds for a silicon atom linked with a carbon atom [29,49–51]. The presence of the $T^n$ contribution in the $^{29}$Si CP-MAS NMR spectrum confirms that APTES was grafted on silica nanoparticles surface.

### 3.5. Synthesis of PDLLA-grafted silica nanoparticles (Np-PDLLA)

As mentioned previously, the amino-functionalized silica Np were covalently functionalized by the $PDLLA_{5.2K}$–COO–NHS polymer. Indeed, PDLLA chains were attached to the Np by conjugating the NHS-activated carboxyl end-group of $PDLLA_{5.2K}$–COO–NHS to the amino-functionalized silica Np (Scheme 2). The washing of resulting nanoparticles with toluene and ethyl acetate permitted the removal of non-grafted $PDLLA_{5.2K}$–COO–NHS chains, ensuring that there were no free PDLLA chains remaining. Only $PDLLA_{5.2K}$-grafted nanoparticles were investigated here, $PDLLA_{2.2K}$–COO–NHS chains have too low molecular weight to be identified by characterization after grafting.

The size of PDLLA-grafted Np was analyzed by both TEM studies and DLS measurements. Image processing performed on Np-PDLLA led to the same size of Np (359 ± 24 nm) with a narrow polydispersity (*PdI* = 0.004), whereas DLS measurements showed an increase of Np-PDLLA hydrodynamic diameter (890 ± 38 nm) and higher polydispersity index (*PdI* = 0.312) compared to initial silica Np (383 ± 1 nm, *PdI* = 0.096) (Table 3). These diameter and polydispersity index increases are

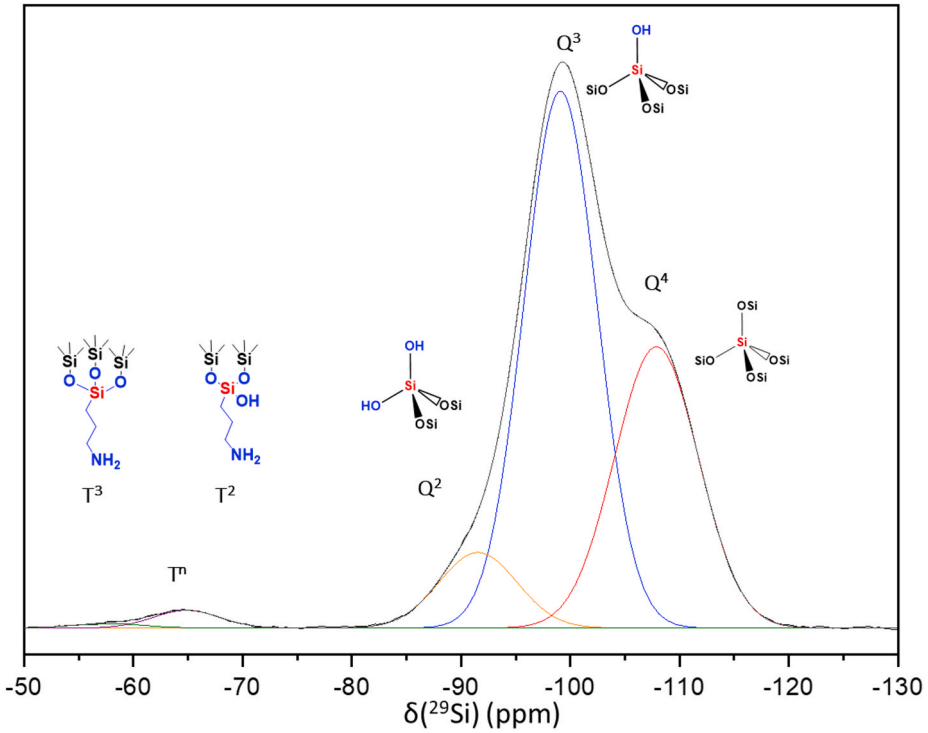


**Fig. 4.** $^{29}$Si CP-MAS SS NMR spectrum of amino-functionalized nanoparticles (Np-$NH_2$).

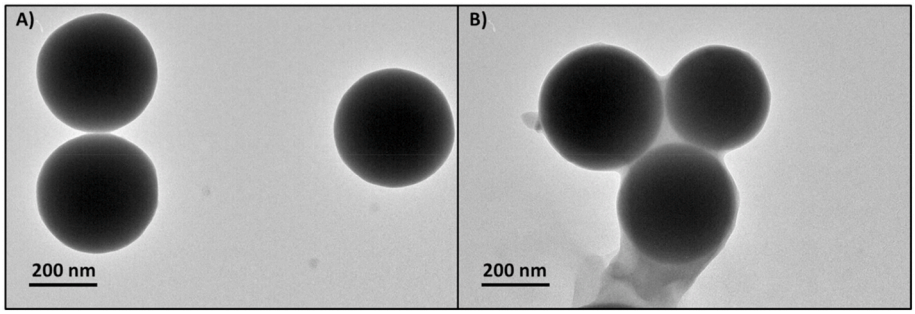


**Fig. 5.** TEM observation of A) initial silica nanoparticles (Np) and B) PDLLA-grafted nanoparticles (Np-PDLLA).

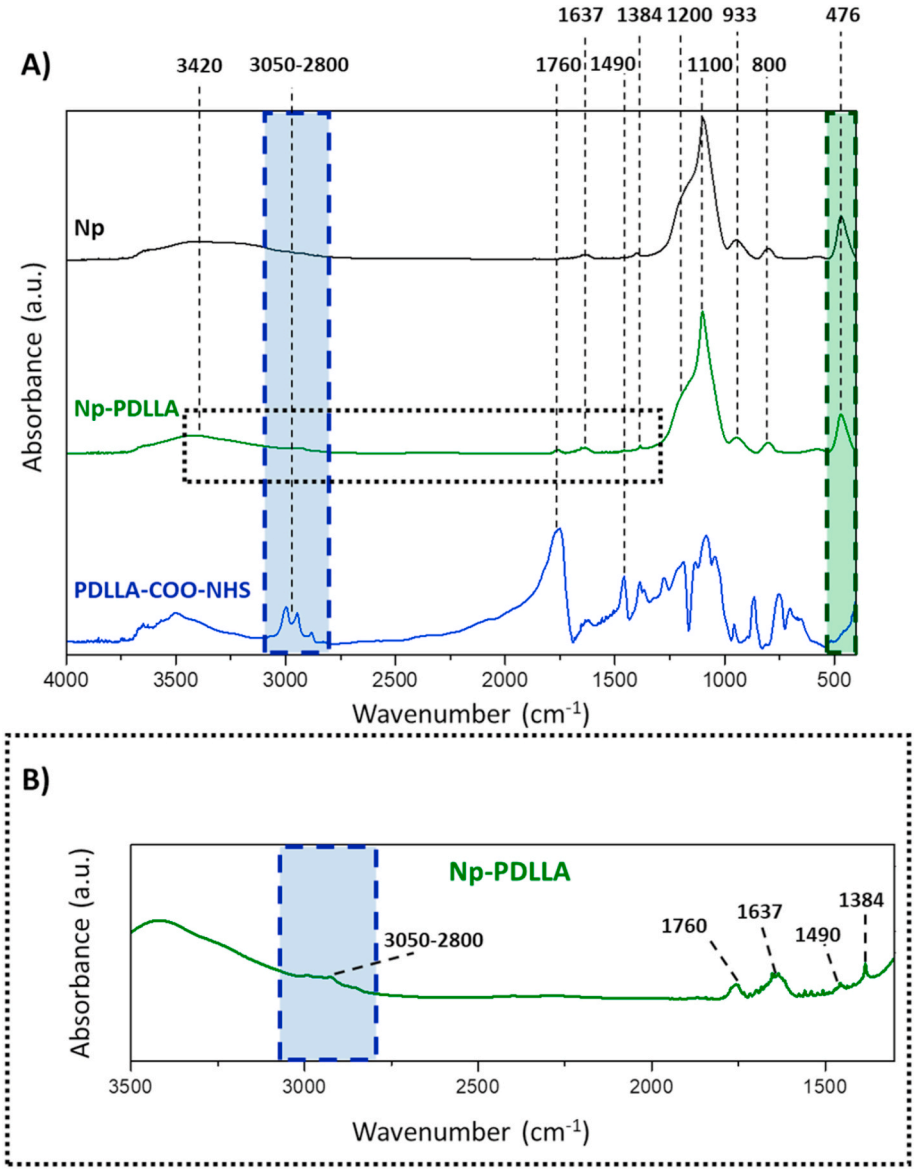


**Fig. 6.** A) FTIR spectrum of initial nanoparticles (Np), PDLLA-grafted nanoparticles (Np-PDLLA) and PDLLA–COO–NHS, B) zoom of Np-PDLLA spectrum in the 3500-1300 $cm^{-1}$ range.

related to the PDLLA grafting onto nanoparticles surface. In fact, when in suspension, the PDLLA corona on silica nanoparticles is swelled by the solvent (EtOH during DLS measurements) [52]. This phenomenon significantly enhances the hydrodynamic diameter. Moreover, the PDLLA layer tends to favor aggregation phenomena due to polymer chains entanglement. ζ-potential of Np-PDLLA was measured (Table 4) and showed a decrease with a sign modification compared to Np-$NH_2$. In fact, Np-PDLLA presents a ζ-potential of $-18 \pm 1$ mV whereas Np-$NH_2$ ζ potential is $14 \pm 1$ mV. The sign modification of PDLLA-grafted nanoparticles ζ-potential is an additional proof of surface modification. TEM

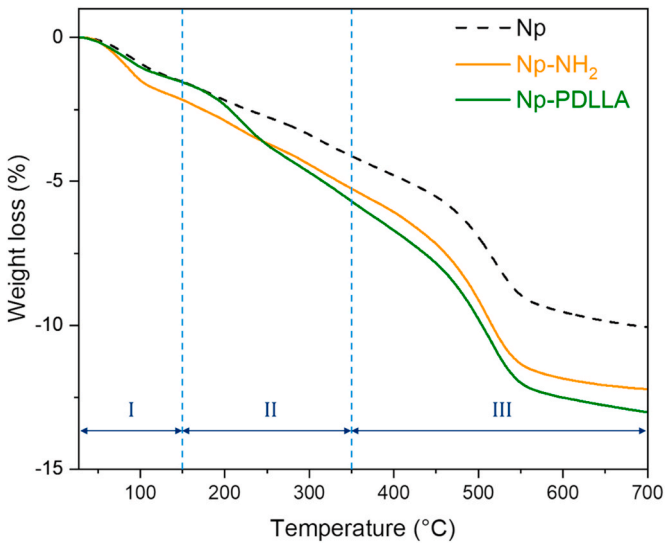


**Fig. 7.** TGA curves of initial nanoparticles (Np), amino-functionalized nanoparticles (Np-$NH_2$) and PDLLA-grafted nanoparticles (Np-PDLLA).

observation of initial and Np-PDLLA at high magnification (x10 000) showed the presence of the polymer corona around silica nanoparticles and the Np aggregation phenomenon (Fig. 5).

FTIR spectroscopic analysis of Np, PDLLA–COO–NHS and Np-PDLLA also confirmed the presence of PDLLA grafted on nanoparticles surface. As shown on Fig. 6, the spectrum of the initial silica nanoparticles presents the characteristic absorption bands of silica [29,53,54]. Band at 3420 $cm^{-1}$ is assigned to stretching, the vibration at 1100 $cm^{-1}$ to the asymmetric stretching, and the band at 933 $cm^{-1}$ to the asymmetric bending of silanol groups (Si–OH). The vibrations at 476 $cm^{-1}$, 800 $cm^{-1}$ and the shoulder at 1200 $cm^{-1}$ correspond respectively to asymmetric bending, symmetric vibration and asymmetric stretching of siloxane groups (Si–O–Si). Absorption bands at 1637 $cm^{-1}$ is linked to residual intermolecular water and the one at 1384 $cm^{-1}$ is due to *Si*–$CH_2$ stretching (pollution). As expected for an organic compound, the number of bands is significantly higher for the PDLLA–COO–NHS spectrum. Then, we focused on most intense and characteristic bands. Absorption bands at 2800-3050 $cm^{-1}$ and 1490 $cm^{-1}$ are ascribed to stretching vibration of –CH and –$CH_3$ groups and to bending vibration of –CH groups. The most typical vibration of PDLLA is the stretching vibration of carbonyl groups (–C═O) at 1760 $cm^{-1}$ [35]. Np-PDLLA spectrum presents all characteristic absorption bands of silica nanoparticles. Moreover, a thorough observation (Fig. 6B) highlights the presence of typical vibration of PDLLA–COO–NHS at 1760 $cm^{-1}$ from carbonyl groups, as well as a low contribution at 3050-2800 $cm^{-1}$ and 1490 $cm^{-1}$ from –CH and –$CH_3$ groups. Those vibrations allow confirming the covalent grafting of PDLLA–COO–NHS at the silica nanoparticle surface.

The silica surface functionalization with amine and PDLLA was also highlighted by TGA analyses. TGA curves (Fig. 7) of initial Np, amino-functionalized Np (Np-$NH_2$) and PDLLA-grafted Np (Np-PDLLA) exhibit three domains. The first domain (I) ending around 150 °C is characteristic of adsorbed water release; the second domain (II) going approximately up to 350 °C is ascribed to external OH groups dehydroxylation overlapped with PDLLA degradation and the third domain (III) ending at around 700 °C is linked to the degradation of alkoxysilane from APTES and internal OH groups [27,35,39,55]. The different weight losses, measured depending on the type of sample, demonstrate the presence of alkoxysilane (−7.1 wt%, domain III) on Np-$NH_2$ and alkoxysilane (−7.3 wt%, domain III) and PDLLA–COO–NHS (−4.2 wt%, domain II) on PDLLA-Np surface.

### 3.6. *Dual approach for grafting quantification*

In this study, we developed quantitative methods to evaluate the amount of alkoxysilane presents on nanoparticles surface and the quantity of customized $PDLLA_{5.2K}$–COO–NHS grafted on amino-functionalized nanoparticles. Those methods were based on calibration with mechanical mixtures of known composition of Np and APTES on the one hand, and Np and PDLLA on the other hand. Five calibration compositions of [Np]:[APTES] and [Np]:[PDLLA] were prepared for APTES quantification and PDLLA quantification respectively. The chosen ratio were 100:0; 70:30; 50:50; 30:70 and 0:100 for both types of calibration samples. Firstly, condensate APTES or PDLLA amounts were mixed with initial silica Np in an agate mortar. Then, mixed samples were placed overnight in oven at 60 °C. The samples were finally crushed before analysis.

For APTES quantification, we used TGA weight loss measurements. Calibration samples were characterized by TGA, following the same program and parameters than for Np, Np-$NH_2$ and Np-PDLLA analysis. Due to the limited amount of calibration samples, only two of them (70:30 and 30:70) were analyzed twice in order to check for reproducibility (Figure S4). This analysis allowed us to determine a calibration curve (Figure S4) based on weight loss between 350 °C and 700 °C and to evaluate more precisely the quantity of grafted carbon chains (CNH) from alkoxysilane present at nanoparticles surface. For Np-$NH_2$, the CNH quantity represents 27 ± 1 mmol; it corresponds to a density of 12 ± 1 grafted CNH/$nm^2$ combining Eq. (3) and Eq. (4), which is equivalent to the grafted quantity of alkoxysilane. For Np-PDLLA the amount of grafted CNH determined was 31 ± 2 mmol, corresponding to 14 ± 1 grafted carbon chains (CNH)/$nm^2$ (Eq. (3) and Eq. (4)).

$$m(\mathrm{Np}) = 100 - [n(CNH) \cdot M(SiO_3CNH)] \quad (3)$$

$$Grafting\ \ density = [n(CNH) \cdot N_A]/_{[m(Np) \cdot SSA]} \quad (4)$$

With m(Np) the percentage of mass of NpSi (wt %) present in the sample, n(CNH) the quantity of grafted CNH chains (mol), M($SiO_3$CNH) the molar mass of grafted alkoxysilane (134 g.$mol^{-1}$), $N_A$ the Avogadro constant and SSA the Np specific surface area ($m^2$/g).

The same method was followed to evaluate the amount of PDLLA

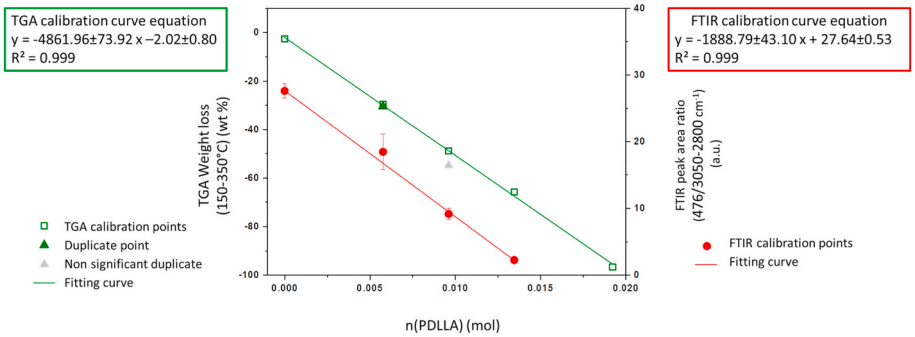


**Fig. 8.** Calibration curves from the dual approach quantification methods allowing the determination of PDLLA quantity (mol) grafted on silica nanoparticles. In green, the calibration points and fitting curve based on TGA weight loss measurements (150–350 °C); in red, calibration points and fitting curve based on peak area ratio (476/3050-2800 $cm^{-1}$) from FTIR spectroscopy data analysis. (For interpretation of the references to colour in this figure legend, the reader is referred to the Web version of this article.)

grafted on Np-PDLLA by TGA. In this case, the calibration curve (Fig. 8) was built using the weight loss between 150 °C and 350 °C. Two compositions were analyzed in duplicate: 70:30 and 50:50. The duplicate of 50:50 composition was found to be not significant (grey triangle on Fig. 8); it was excluded from the calibration curve. The determined quantity of PDLLA grafted is 0.44 ± 0.05 mmol corresponding to a grafting density of 0.20 ± 0.02 chain of PDLLA/nm$^2$ (Eq. (4) and Eq. (5)).

$$\mathrm{m(Np)} = 100 - [n(CNH) \cdot M(SiO_3CNH)] - n(PDLLA) \cdot M_n(PDLLA) \quad (5)$$

With n(PDLLA) and $M_n$(PDLLA) respectively the determined quantity (mol) of grafted PDLLA and PDLLA molecular weight (g.mol$^{-1}$).

A second method was used to confirm the quantification of PDLLA grafting on Np-PDLLA via the peak area ratio calculated from FTIR spectroscopic data. The previously prepared calibration samples were analyzed by FTIR spectroscopy (KBr pellets, transmission mode), three pellets were characterized for each sample. After applying the same baseline processing for all sample spectra, we performed a spectral decomposition. Peak areas were measured for band at 476 cm$^{-1}$ (characteristic of silica Np) which remains unmodified after grafting contrary to Si–OH related bands and 3050-2800 cm$^{-1}$ (characteristic of PDLLA). We focused our study on those bands (presented in blue and green area on Fig. 6) because they did not present overlapping with other bands and were easier to isolate. The ratio between the 476 cm$^{-1}$ and the 3050-2800 cm$^{-1}$ band area were calculated and permitted to plot the calibration curve (Fig. 8). The quantity of grafted PDLLA evaluated by this method is 0.37 ± 0.05 mmol, corresponding to 0.16 ± 0.02 chain of grafted PDLLA/nm$^2$. However, the grafting density evaluation using FTIR spectroscopy approach is less precise than by TGA. In fact, only the mass of grafted PDLLA is used to evaluate the amount of Np initially present (Eq. (5)) as it is not possible to quantify grafted alkoxysilane by this method.

These two quantitative methods (TGA and FTIR spectroscopy) led to the determination of equivalent quantities of grafted PDLLA on Np-PDLLA. The obtained grafting density are similar, but FTIR spectroscopy approach uncertainty must be considered. Each method presents some limitations, which is why this dual approach is interesting to validate the quantification of grafted PDLLA. In fact quantification based on TGA weight loss seems to be more precise but only two samples were analyzed in duplicate. Additional calibration samples should be used to further develop this promising quantitative method. Although it is faster than TGA method, the method based on FTIR peak area ratio does not allow the evaluation of the exact grafting density as the grafted alkoxysilane quantity cannot be determined. Moreover, with this calibration curve it is not possible to quantify PDLLA grafted quantities higher than 70 wt% without extrapolation.

The grafting density may appear low comparing to grafted alkoxysilane density but considering the steric hindrance effect, results are consistent with the molecular weight of the polymer chains. To the best of our knowledge, it is the first time that such a multi-tool approach is used to quantify grafted PDLLA. Moreover, if we use the quantification method of Wu et al. the grafting density for Np-PDLLA is 0.13 PDLLA chains/nm$^2$ [35]. Comparing to this study and for the same molecular weight, this value is close to the one evaluated for the “grafting from” method (0.38 chains/nm$^2$) and significantly higher than the one obtained for the “grafting to” method (0.022 chains/nm$^2$).

Therefore, we developed an innovative technique to obtain PDLLA-grafted silica nanoparticles using customized PDLLA polymer chains grafted onto silica surface, leading to well-defined and precisely characterized grafted nanoparticles that can be used as composite nanofillers.

## 4. Conclusion

This study aimed to develop PDLLA grafted silica nanoparticles using a “grafting to” method, and to characterize and quantify precisely the grafting. The most compelling result was the demonstration for the first time that well-defined PDLLA chains can be grafted onto controlled size silica nanoparticles surface. Different techniques were used to confirm the good grafting of PDLLA–COO–NHS chains onto nanoparticles surface and gave a precise characterization of the PDLLA-grafted silica nanoparticles. The results presented in this work showed a proof of controlled “grafting onto” concept and an increase of interactions between PDLLA-grafted nanoparticles compared to initial silica nanoparticles. Moreover, precise quantification of PDLLA grafted amount was performed thank to the development of a dual approach based on two different techniques converging to a similar result. However, this multi-tool quantification method could be improved by multiplying calibration samples analysis and ratios to have a greater quantification range. This preliminary work demonstrated how to produce PDLLA-grafted silica nanoparticles in order to be used as composite nanofillers and worth further development. The results of this study could also have greater implications in the development of composite biomaterials, permitting the elaboration of performant PDLLA/silica Np biomedical composite scaffolds. The use of as-prepared PDLLA-grafted silica Np as fillers in composite materials is expected to improve fillers dispersion state and interaction with the polymer matrix, and thus increase processability, homogeneity and mechanical properties, of final scaffolds, these three properties being crucial for their bio-integration.

## CRediT authorship contribution statement

**Prescillia Lagarrigue:** Investigation, Methodology, Validation, Writing - Original draft. **Jérémy Soulié:** Co-supervision, Conceptualization, Validation, Resources, Methodology, Funding acquisition, Writing – Original draft. **David Grossin:** Validation, Writing - Original draft. **Agnès Dupret-Bories:** Writing - Review & Editing.

*Christèle Combes:* Co-supervision, Validation, Project administration, Funding acquisition, Writing - Original draft.

*Vincent Darcos:* Supervision, Conceptualization, Methodology, Resources, Project administration, Funding acquisition, Writing - Original draft.


## Funding

This work was supported by the Institut Carnot Chimie Balard Cirimat.


## CRediT authorship contribution statement

**Prescillia Lagarrigue:** Investigation, Methodology, Validation, Writing - original draft. **Jérémy Soulié:** Supervision, Conceptualization, Validation, Resources, Methodology, Funding acquisition, Writing - original draft. **David Grossin:** Validation, Writing - original draft. **Agnès Dupret-Bories:** Writing - review & editing. **Christèle Combes:** Supervision, Validation, Project administration, Funding acquisition, Writing - original draft. **Vincent Darcos:** Supervision, Conceptualization, Methodology, Resources, Project administration, Funding acquisition, Writing - original draft.

## Declaration of competing interest

The authors declare that they have no known competing financial interests or personal relationships that could have appeared to influence the work reported in this paper.


## Acknowledgments

The authors thank the Institut Carnot Chimie Balard Cirimat for supporting this work and the SynBio3 platform (IBMM Montpellier) for SEC analysis.

## Appendix A. Supplementary data

Supplementary data to this article can be found online at https://doi.org/10.1016/j.polymer.2020.123048.

## References


[1] M.R. Brinker, D.P. O'Connor, The incidence of fractures and dislocations referred for orthopaedic services in a capitated population, J. Bone Jt. Surg. 86 (2004) 290–297, https://doi.org/10.2106/00004623-200402000-00011.

[2] B. Baroli, From natural bone grafts to tissue engineering therapeutics: brainstorming on pharmaceutical formulative requirements and challenges, J. Pharmacol. Sci. 98 (2009) 1317–1375, https://doi.org/10.1002/jps.21528.

[3] S.K. Nandi, S. Roy, P. Mukherjee, B. Kundu, D.K. De, D. Basu, Orthopaedic applications of bone graft & graft substitutes: a review, Indian J. Med. Res. 132 (2010) 15–30.

[4] K. Rezwan, Q.Z. Chen, J.J. Blaker, A.R. Boccaccini, Biodegradable and bioactive porous polymer/inorganic composite scaffolds for bone tissue engineering, Biomaterials 27 (2006) 3413–3431, https://doi.org/10.1016/j.biomaterials.2006.01.039.

[5] H. Qu, H. Fu, Z. Han, Y. Sun, Biomaterials for bone tissue engineering scaffolds: a review, RSC Adv. 9 (2019) 26252–26262, https://doi.org/10.1039/C9RA05214C.

[6] E. Salernitano, C. Migliaresi, Composite materials for biomedical applications: a review, J. Appl. Biomater. Biomech. 1 (2003) 3–18, https://doi.org/10.1177/228080003000100102.

[7] S. Ramakrishna, J. Mayer, E. Wintermantel, K.W. Leong, Biomedical applications of polymer-composite materials: a review, Compos. Sci. Technol. 61 (2001) 1189–1224, https://doi.org/10.1016/S0266-3538(00)00241-4.

[8] F. Baino, S. Fiorilli, C. Vitale-Brovarone, Composite biomaterials based on sol-gel mesoporous silicate glasses: a review, Bioengineering 4 (2017) 1–18, https://doi.org/10.3390/bioengineering4010015.

[9] M.M. Stevens, Biomaterials for bone tissue engineering, Mater. Today 11 (2008) 18–25, https://doi.org/10.1016/S1369-7021(08)70086-5.

[10] B.L. Seal, T.C. Otero, A. Panitch, Polymeric biomaterials for tissue and organ regeneration, Mater. Sci. Eng. R Rep. 34 (2001) 147–230, https://doi.org/10.1016/S0927-796X(01)00035-3.

[11] D.W. Hutmacher, Scaffolds in tissue engineering bone and cartilage, Biomaterials 21 (2000) 2529–2543, https://doi.org/10.1016/S0142-9612(00)00121-6.

[12] M. Schardosim, J. Soulié, D. Poquillon, S. Cazalbou, B. Duployer, C. Tenailleau, C. Rey, R. Hübler, C. Combes, Freeze-casting for PLGA/carbonated apatite composite scaffolds: structure and properties, Mater. Sci. Eng. C 77 (2017) 731–738, https://doi.org/10.1016/j.msec.2017.03.302.

[13] A.R. Boccaccini, J.J. Blaker, V. Maquet, R.M. Day, R. Jérôme, Preparation and characterisation of poly(lactide-co-glycolide) (PLGA) and PLGA/Bioglass® composite tubular foam scaffolds for tissue engineering applications, Mater. Sci. Eng. C 25 (2005) 23–31, https://doi.org/10.1016/j.msec.2004.03.002.

[14] H. Maleki, M.-A. Shahbazi, S. Montes, S.H. Hosseini, M.R. Eskandari, S. Zaunschirm, T. Verwanger, S. Mathur, B. Milow, B. Krammer, N. Hüsing, Mechanically strong silica-silk fibroin bioaerogel: a hybrid scaffold with ordered honeycomb micromorphology and multiscale porosity for bone regeneration, ACS Appl. Mater. Interfaces 11 (2019) 17256–17269, https://doi.org/10.1021/acsami.9b04283.

[15] C.E. Plazas Bonilla, S. Trujillo, B. Demirdögen, J.E. Perilla, Y. Murat Elcin, J. L. Gómez Ribelles, New porous polycaprolactone–silica composites for bone regeneration, Mater. Sci. Eng. C 40 (2014) 418–426, https://doi.org/10.1016/j.msec.2014.04.024.

[16] W. Heidemann, S. Jeschkeit, K. Ruffieux, J.H. Fischer, M. Wagner, G. Krüger, E. Wintermantel, K.L. Gerlach, Degradation of poly(d, l)lactide implants with or without addition of calciumphosphates in vivo, Biomaterials 22 (2001) 2371–2381, https://doi.org/10.1016/S0142-9612(00)00424-5.

[17] H. Cai, V. Dave, R.A. Gross, S.P. McCarthy, Effects of physical aging, crystallinity, and orientation on the enzymatic degradation of poly(lactic acid), J. Polym. Sci., Part B: Polym. Phys. 34 (1996) 2701–2708, https://doi.org/10.1002/(SICI)1099-0488(19961130)34:16<2701::AID-POLB2>3.0.CO;2-S.

[18] S.M. Li, H. Garreau, M. Vert, Structure-property relationships in the case of the degradation of massive aliphatic poly-(α-hydroxy acids) in aqueous media: Part 1: poly(d,l-lactic acid), J. Mater. Sci. Mater. Med. 1 (1990) 123–130, https://doi.org/10.1007/BF00700871.

[19] E.M. Carlisle, Silicon: a requirement in bone formation independent of vitamin D1, Calcif, Tissue Int 33 (1981) 27–34, https://doi.org/10.1007/BF02409409.

[20] D.M. Reffitt, N. Ogston, R. Jugdaohsingh, H.F.J. Cheung, B.A.J. Evans, R.P. H. Thompson, J.J. Powell, G.N. Hampson, Orthosilicic acid stimulates collagen type 1 synthesis and osteoblastic differentiation in human osteoblast-like cells in vitro, Bone 32 (2003) 127–135, https://doi.org/10.1016/S8756-3282(02)00950-X.

[21] I.A. Rahman, V. Padavettan, Synthesis of silica nanoparticles by sol-gel: size-dependent properties, surface modification, and applications in silica-polymer nanocomposites—a review, J. Nanomater. 2012 (2012) 1–15, https://doi.org/10.1155/2012/132424.

[22] J.-W. Huang, Y. Chang Hung, Y.-L. Wen, C.-C. Kang, M.-Y. Yeh, Polylactide/nano- and micro-scale silica composite films. II. Melting behavior and cold crystallization, J. Appl. Polym. Sci. 112 (2009) 3149–3156, https://doi.org/10.1002/app.29699.

[23] S.K. Misra, D. Mohn, T.J. Brunner, W.J. Stark, S.E. Philip, I. Roy, V. Salih, J. C. Knowles, A.R. Boccaccini, Comparison of nanoscale and microscale bioactive glass on the properties of P(3HB)/Bioglass® composites, Biomaterials 29 (2008) 1750–1761, https://doi.org/10.1016/j.biomaterials.2007.12.040.

[24] T.C. Huang, J.M. Yeh, J.C. Yang, Effect of silica size on the thermal, mechanical and biodegradable properties of polylactide/silica composite material prepared by melt blending, Adv. Mater. Res. 123–125 (2010) 1215–1218. https://doi.org/10.4028/www.scientific.net/AMR.123-125.1215.

[25] S.C. Jana, S. Jain, Dispersion of nanofillers in high performance polymers using reactive solvents as processing aids, Polymer 42 (2001) 6897–6905.

[26] W.R. Lenart, M.J.A. Hore, Structure–property relationships of polymer-grafted nanospheres for designing advanced nanocomposites, Nano-Struct. Nano-Objects 16 (2018) 428–440, https://doi.org/10.1016/j.nanoso.2017.11.005.

[27] A. El-Fiqi, T.-H. Kim, M. Kim, M. Eltohamy, J.-E. Won, E.-J. Lee, H.-W. Kim, Capacity of mesoporous bioactive glass nanoparticles to deliver therapeutic molecules, Nanoscale 4 (2012) 7475–7488, https://doi.org/10.1039/c2nr31775c.

[28] A.S. Morris, A. Adamcakova-Dodd, S.E. Lehman, A. Wongrakpanich, P.S. Thorne, S. C. Larsen, A.K. Salem, Amine modification of nonporous silica nanoparticles reduces inflammatory response following intratracheal instillation in murine lungs, Toxicol. Lett. 241 (2016) 207–215, https://doi.org/10.1016/j.toxlet.2015.11.006.

[29] I.A. Rahman, M. Jafarzadeh, C.S. Sipaut, Synthesis of organo-functionalized nanosilica via a co-condensation modification using γ-aminopropyltriethoxysilane (APTES), Ceram. Int. 35 (2009) 1883–1888, https://doi.org/10.1016/j.ceramint.2008.10.028.

[30] B. Qiao, T.-J. Wang, H. Gao, Y. Jin, High density silanization of nano-silica particles using γ-aminopropyltriethoxysilane (APTES), Appl. Surf. Sci. 351 (2015) 646–654, https://doi.org/10.1016/j.apsusc.2015.05.174.

[31] Y. Li, X.S. Sun, Preparation and characterization of polymer−inorganic nanocomposites by in situ melt polycondensation of l-lactic acid and surface-hydroxylated MgO, Biomacromolecules 11 (2010) 1847–1855, https://doi.org/10.1021/bm100320q.

[32] Y.-B. Luo, X.-L. Wang, D.-Y. Xu, Y.-Z. Wang, Preparation and characterization of poly(lactic acid)-grafted TiO2 nanoparticles with improved dispersions, Appl. Surf. Sci. 255 (2009) 6795–6801, https://doi.org/10.1016/j.apsusc.2009.02.074.

[33] L. Wu, D. Cao, Y. Huang, B.-G. Li, Poly(l-lactic acid)/$SiO_2$ nanocomposites via in situ melt polycondensation of l-lactic acid in the presence of acidic silica sol: preparation and characterization, Polymer 49 (2008) 742–748, https://doi.org/10.1016/j.polymer.2007.12.019.

[34] M. Joubert, C. Delaite, E. Bourgeat-Lami, P. Dumas, Ring-opening polymerization of ε-caprolactone and l-lactide from silica nanoparticles surface, J. Polym. Sci. Part Polym. Chem. 42 (2004) 1976–1984, https://doi.org/10.1002/pola.20035.

[35] F. Wu, B. Zhang, W. Yang, Z. Liu, M. Yang, Inorganic silica functionalized with PLLA chains via grafting methods to enhance the melt strength of PLLA/silica nanocomposites, Polymer 55 (2014) 5760–5772, https://doi.org/10.1016/j.polymer.2014.08.070.

[36] F. Wu, B. Zhang, W. Yang, Z. Liu, M. Yang, Inorganic silica functionalized with PLLA chains via grafting methods to enhance the melt strength of PLLA/silica nanocomposites, Polymer 55 (2014) 5760–5772, https://doi.org/10.1016/j.polymer.2014.08.070.

[37] C. Chevigny, F. Dalmas, E. Di Cola, D. Gigmes, D. Bertin, F. Boué, J. Jestin, Polymer-grafted-nanoparticles nanocomposites: dispersion, grafted chain conformation, and rheological behavior, Macromolecules 44 (2011) 122–133, https://doi.org/10.1021/ma101332s.

[38] S. Yan, J. Yin, Y. Yang, Z. Dai, J. Ma, X. Chen, Surface-grafted silica linked with L-lactic acid oligomer: a novel nanofiller to improve the performance of biodegradable poly(l-lactide), Polymer 48 (2007) 1688–1694, https://doi.org/10.1016/j.polymer.2007.01.037.

[39] F. Wu, X. Lan, D. Ji, Z. Liu, W. Yang, M. Yang, Grafting polymerization of polylactic acid on the surface of nano-$SiO_2$ and properties of PLA/PLA grafted-$SiO_2$ nanocomposites, J. Appl. Polym. Sci. 129 (2013) 3019–3027, https://doi.org/10.1002/app.38585.

[40] D.-W. Shi, X.-L. Lai, Y.-P. Jiang, C. Yan, Z.-Y. Liu, W. Yang, M.-B. Yang, Synthesis of inorganic silica grafted three-arm PLLA and their behaviors for PLA matrix, Chin. J. Polym. Sci. 37 (2019) 216–226, https://doi.org/10.1007/s10118-019-2191-6.

[41] W. Stöber, A. Fink, E. Bohn, Controlled growth of monodisperse silica spheres in the micron size range, J. Colloid Interface Sci. 26 (1968) 62–69, https://doi.org/10.1016/0021-9797(68)90272-5.

[42] S.-H. Lee, S.H. Kim, Y.-K. Han, Y.H. Kim, Synthesis and degradation of end-group-functionalized polylactide, J. Polym. Sci. Part Polym. Chem. 39 (2001) 973–985.

[43] A. El-Fiqi, J.H. Lee, E.-J. Lee, H.-W. Kim, Collagen hydrogels incorporated with surface-aminated mesoporous nanobioactive glass: improvement of physicochemical stability and mechanical properties is effective for hard tissue engineering, Acta Biomater. 9 (2013) 9508–9521, https://doi.org/10.1016/j.actbio.2013.07.036.

[44] S.M. Guillaume, M. Schappacher, A. Soum, Polymerization of ε-caprolactone initiated by Nd(BH4)3(THF)3: synthesis of hydroxytelechelic poly(ε-caprolactone), Macromolecules 36 (2003) 54–60, https://doi.org/10.1021/ma020993g.

[45] Y. Hu, V. Darcos, S. Monge, S. Li, Synthesis and self-assembling of poly(N-isopropylacrylamide)-block-poly(L-lactide)-block-poly(N-isopropylacrylamide) triblock copolymers prepared by combination of ring-opening polymerization and atom transfer radical polymerization, J. Polym. Sci. Part Polym. Chem. 51 (2013) 3274–3283, https://doi.org/10.1002/pola.26721.

[46] K.S. Lim, M.H. Alves, L.A. Poole-Warren, P.J. Martens, Covalent incorporation of non-chemically modified gelatin into degradable PVA-tyramine hydrogels, Biomaterials 34 (2013) 7097–7105, https://doi.org/10.1016/j.biomaterials.2013.06.005.

[47] J.R. Jones, Review of bioactive glass: from Hench to hybrids, Acta Biomater. 9 (2013) 4457–4486, https://doi.org/10.1016/j.actbio.2012.08.023.
[48] R. Watanabe, T. Yokoi, E. Kobayashi, Y. Otsuka, A. Shimojima, T. Okubo, T. Tatsumi, Extension of size of monodisperse silica nanospheres and their well-ordered assembly, J. Colloid Interface Sci. 360 (2011) 1–7, https://doi.org/10.1016/j.jcis.2010.09.001.
[49] G.Stephen Caravajal, D.E. Leyden, G.R. Quinting, G.E. Maciel, Structural characterization of (3-aminopropyl)triethoxysilane-modified silicas by silicon-29 and carbon-13 nuclear magnetic resonance, Anal. Chem. 60 (1988) 1776–1786, https://doi.org/10.1021/ac00168a027.
[50] R.A. Martin, S. Yue, J.V. Hanna, P.D. Lee, R.J. Newport, M.E. Smith, J.R. Jones, Characterizing the hierarchical structures of bioactive sol-gel silicate glass and hybrid scaffolds for bone regeneration, Philos. Trans. R. Soc. Math. Phys. Eng. Sci. 370 (2012) 1422–1443, https://doi.org/10.1098/rsta.2011.0308.
[51] S.L. Greasley, S.J. Page, S. Sirovica, S. Chen, R.A. Martin, A. Riveiro, J.V. Hanna, A. E. Porter, J.R. Jones, Controlling particle size in the Stöber process and incorporation of calcium, J. Colloid Interface Sci. 469 (2016) 213–223, https://doi.org/10.1016/j.jcis.2016.01.065.
[52] C. Chevigny, J. Jestin, D. Gigmes, R. Schweins, E. Di-Cola, F. Dalmas, D. Bertin, F. Boué, "Wet-to-dry" conformational transition of polymer layers grafted to nanoparticles in nanocomposite, Macromolecules 43 (2010) 4833–4837, https://doi.org/10.1021/ma100858h.
[53] I.A. Rahman, P. Vejayakumaran, C.S. Sipaut, J. Ismail, C.K. Chee, Size-dependent physicochemical and optical properties of silica nanoparticles, Mater. Chem. Phys. 114 (2009) 328–332, https://doi.org/10.1016/j.matchemphys.2008.09.068.
[54] S. Rovani, J.J. Santos, P. Corio, D.A. Fungaro, An alternative and simple method for the preparation of bare silica nanoparticles using sugarcane waste ash, an abundant and despised residue in the Brazilian industry, J. Braz. Chem. Soc. 30 (2019) 1524–1533, https://doi.org/10.21577/0103-5053.20190049.
[55] R. Mueller, H.K. Kammler, K. Wegner, S.E. Pratsinis, OH surface density of $SiO_2$ and $TiO_2$ by thermogravimetric analysis, Langmuir 19 (2003) 160–165, https://doi.org/10.1021/la025785w.